Title
NPAS1 represses the generation of specific subtypes of cortical interneurons.

Journal
Neuron, 84(5)

ISSN
0896-6273

Authors
Stanco, Amelia
Pla, Ramón
Vogt, Daniel
et al.

Publication Date
2014-12-01

DOI
10.1016/j.neuron.2014.10.040

Peer reviewed

Published in final edited form as:
Neuron. 2014 December 3; 84(5): 940–953. doi:10.1016/j.neuron.2014.10.040.

NPAS1 Represses the Generation of Specific Subtypes of Cortical Interneurons

Amelia Stanco[1,*], **Ramón Pla**[1,6], **Daniel Vogt**[1,6], **Yiran Chen**[2], **Shyamali Mandal**[1,†], **Jamie Walker**[3], **Robert F. Hunt**[4], **Susan Lindtner**[1], **Carolyn A. Erdman**[1], **Andrew A. Pieper**[5], **Steven P. Hamilton**[1,‡], **Duan Xu**[2], **Scott C. Baraban**[4], and **John L. R. Rubenstein**[1,*]

[1]Department of Psychiatry, Neuroscience Program and the Nina Ireland Laboratory of Developmental Neurobiology, University of California San Francisco, San Francisco, CA 94158-2324, USA

[2]Department of Radiology and Biomedical Imaging, University of California San Francisco, San Francisco, CA 94143, USA

[3]Department of Biochemistry, UT Southwestern Medical Center, Dallas, TX 75390, USA

[4]Department of Neurological Surgery, Neuroscience Program, University of California San Francisco, San Francisco, CA 94143, USA

[5]Department of Psychiatry and Neurology, University of Iowa Carver College of Medicine, Iowa City, IA 52242, USA

Summary

Little is known about genetic mechanisms that regulate the ratio of cortical excitatory and inhibitory neurons. We show that *NPAS1* and *NPAS3* transcription factors (TF) are expressed in progenitor domains of the mouse basal ganglia (subpallium, MGE and CGE). *NPAS1*$^{-/-}$ mutants had increased proliferation, ERK signaling and expression of *Arx* in the MGE and CGE. *NPAS1*$^{-/-}$ mutants also had increased neocortical inhibition (sIPSC and mIPSC), and generated an excess of somatostatin^{+} (SST) (MGE-derived) and vasoactive intestinal polypeptide^{+} (VIP) (CGE-derived) neocortical interneurons, but had a normal density of parvalbumin^{+} (PV) (MGE-derived) interneurons. In contrast, *NPAS3*$^{-/-}$ mutants showed decreased proliferation and ERK signaling in progenitors of the ganglionic eminences and had fewer SST^{+} and VIP^{+} interneurons. NPAS1 repressed activity of an *Arx* enhancer, and *Arx* over-expression resulted in increased proliferation of CGE progenitors. These results provide novel insights into genetic regulation of cortical interneuron numbers and cortical inhibitory tone.

[*]Correspondence: john.rubenstein@ucsf.edu; amelia.stanco@ucsf.edu.
[6]These authors contributed equally to this work.
[†]Current Address: Genentech, Inc., South San Francisco, CA 94080, USA.
[‡]Current Address: Kaiser Permanente, San Francisco, CA 94118, USA.

Supplemental Information
Supplemental Information includes seven figures, Supplemental Experimental Procedures, and Supplemental Text.

Keywords

NPAS1; NPAS3; Cortical Interneuron Development; Excitation/Inhibition

Introduction

While rapid progress has been made in understanding the regulation of neural regional and cell fate specification, much less is known about genetic mechanisms underlying brain size and how the correct ratios of excitatory and inhibitory neurons within local circuits are generated. Understanding these mechanisms is essential for elucidating important facets of brain development that underlie neurodevelopmental disorders that may have an imbalance of cortical excitation/inhibition (E/I) (e.g. epilepsy, autism spectrum disorders, and schizophrenia) (Lewis et al., 2012; Marin, 2012; Rubenstein and Merzenich, 2003; Yizhar et al., 2011), and to understanding why many autistic children have macrocephaly that includes a large cerebral cortex (Courchesne et al., 2007; Hazlett et al., 2011). While unifying genetic mechanisms which control cortex size and E/I balance have not yet been elucidated, progress has been made in understanding each of these processes individually.

Genetic causes of human neonatal macrocephaly are present in individuals with mutations in genes regulating growth factor signaling, particularly in pathways that engage the function of AKT and PTEN (Poduri et al., 2012; Rivière et al., 2012; Striano and Zara, 2012; Zhou and Parada, 2012), and RAS and MAPK (Gripp et al., 2013). For instance, patients who are heterozygotes for loss of function PTEN mutations have macrocephaly, and are at increased risk for autism (Zhou and Parada, 2012).

Likewise, progress has been made in understanding the mechanisms that control the generation of cortical excitatory and inhibitory neurons (Gelman et al., 2012; Kwan et al., 2012; Marin, 2013), and the mechanisms that coordinate their relative activities to create the proper E/I balance (Le Magueresse and Monyer, 2013). In this regard, there is particular interest in the mechanisms that control the development of cortical inhibitory neurons (GABAergic interneurons). In rodents, most cortical inhibitory neurons are generated during embryogenesis in subpallial structures called the caudal and medial ganglionic eminences (CGE and MGE) (Rudy et al., 2011).

The specification, migration and differentiation of cortical interneurons is controlled by cascades of transcription factors. Some TFs regulate the development of either CGE or MGE derived neurons. For instance, *Lhx6*, *Nkx2-1*, *Olig1* and *Sox6* regulate for the specification and differentiation of MGE derived interneurons (Azim et al., 2009; Batista-Brito et al., 2009; Liodis et al., 2007; Silbereis et al., 2014; Sussel et al., 1999; Zhao et al., 2008). Other TF's, such as the *Arx* and *Dlx* genes, control development of both CGE and MGE derived interneurons (Cobos et al., 2005; Colasante et al., 2008; Marsh et al., 2009).

Herein, we present evidence that the mouse *NPAS* basic helix-loop-helix (bHLH)-PAS TF genes (Erbel-Sieler et al., 2004; Pieper et al., 2005; Zhou et al., 1997) are novel regulators of cortex size and E/I balance. *NPAS1* and *NPAS3* are expressed in telencephalic progenitor domains of the cortex, and the CGE and MGE, and later in immature and mature cortical

interneurons (Batista-Brito et al., 2008; Erbel-Seiler et al., 2004; Zhao et al., 2008). Vertebrate *NPAS* function in embryonic neural progenitors may be related to the function of *Trachealess*, the *NPAS Drosophila* homolog. *Trachealess* modulates fibroblast growth factor (FGF) signaling by transcriptional regulation of the FGF receptor (Ohshiro and Saigo, 1997). In the adult mouse hippocampus, *NPAS3* regulates expression of *FGFR1* to control proliferation of hippocampal granule neurons (Pieper et al., 2005). Here, we have found that *NPAS1* negatively regulates proliferation and MAPK signaling in CGE and MGE progenitors, not by regulating FGF receptor expression, but through an unexpected mechanism, repression of *Arx* expression. As a result, *NPAS1*$^{-/-}$ mutants generate excessive cortical interneurons prenatally, which persisted into adulthood. *NPAS1*$^{-/-}$ mutants also had increased neocortical inhibition (sIPSC and mIPSC), and generated an excess of SST^{+} (MGE-derived) and VIP^{+} (CGE-derived) neocortical interneurons, but had normal numbers of PV^{+} (MGE-derived) interneurons. In contrast, *NPAS3*$^{-/-}$ mutants had a complementary phenotype, with reduced proliferation and MAPK signaling in progenitors of the ganglionic eminences, and the postnatal cortex had fewer SST^{+} and VIP^{+} interneurons.

We propose that our analysis of *NPAS1* and *NPAS3* functions in mice provide novel mechanistic insights into human neuropsychiatric disorders, as *NPAS3* dysfunction is implicated in schizophrenia (Kamnasaran et al., 2003; Macintyre et al., 2010). Furthermore, we have identified sporadic non-synonymous mutations in *NPAS1* and *NPAS3* in autistic individuals.

Results

NPAS1 and *NPAS3* Expression During Interneuron Development

The subpallium generates neocortical interneurons (Flandin et al., 2011; Marin, 2012; Rudy et al., 2011). We examined *NPAS1* and *NPAS3* RNA expression by *in situ* hybridization (ISH) at E13.5, E15.5 and P5 (Figure 1), and assessed *NPAS1* and *NPAS3* expression by immunofluorescence at P0, P5, P15, and P30 (Figure 1 and Figures S1 and S2 and Tables S1 and S2). At E13.5, both had pallial and subpallial ventricular zone (VZ) expression. *NPAS1* showed notable expression in the VZ and subventricular zone (SVZ) of the dorsal and ventral MGE, and CGE. By E15.5, *NPAS3* was expressed in the MGE mantle zone; *NPAS1* expression was prominent in the pallial and subpallial SVZ.

Previous studies have described co-expression of NPAS1 or NPAS3 with cortical interneurons using GABA, GAD-67, or calretinin antibodies in the adult mouse brain (Erbel-Sieler et al., 2004). We have extended co-expression analysis of NPAS1 or NPAS3 with various interneuron markers during cortical interneuron development and in the adult (Figure 1 and Figures S1 and S2 and Tables S1 and S2). At P0, *NPAS1* was expressed in neocortical interneurons; ~100% of NPAS1^{+} cells express *GAD67-GFP*; ~30% had MGE-like properties (*Lhx6-GFP*$^{+}$) (Figures 1D and 1F and Figures S1A and S1B). By P5, *NPAS1* and *NPAS3* were expressed in rostro-caudal gradients in neocortical interneurons; we are unaware of other TFs with this property. Virtually all neocortical NPAS1^{+} cells (99 ± 0.29%) and the majority of NPAS3^{+} cells (67 ± 2.94%) expressed *GAD67-GFP* at P5 (Figures S1C and S1D). By P15, NPAS1 and NPAS3 were expressed by a majority of reelin^{+} (NPAS1: 68 ± 2.78%; NPAS3: 79 ± 4.79%) and SST^{+} (NPAS1: 65 ± 1.95%;

NPAS3: 75 ± 0.44%) interneurons. Both NPAS1 and NPAS3 were expressed in a small proportion of PV^+ cells (NPAS1: 6 ± 0.85%) (NPAS3: 13 ± 1.29%) (Figures S1E, S1F, S1H, S1I, S1J, and S1L). At P30, $NPAS1^+$ cells co-expressed reelin, SST, calretinin (CR), or neuropeptide Y (NPY), but rarely co-expressed PV (reelin: 42 ± 1.94%; SST: 36 ± 3.72%; CR: 28 ± 2.89%; NPY: 12 ± 0.70%; PV: 5 ± 1.24%). On the other hand, $NPAS3^+$ was expressed in a large fraction of all interneuron subtypes assayed, including PV (reelin: 74 ± 2.31%; SST: 75 ± 3.52%; CR: 51 ± 1.23%; PV: 43 ± 1.40%) (Figures S2B–S2E and S2G–S2J and data not shown).

Increased Numbers of Neocortical Interneurons in *NPAS1*$^{-/-}$ Mutants

We studied the effect of an NPAS1 null allele (*NPAS1*$^{-/-}$) (Erbel-Sieler et al., 2004) on neocortical interneuron development using a *GAD67-GFP* allele to label all of the interneurons (Tamamaki et al., 2003). By E15.5 there was an increased density of GFP^+ interneurons through the intermediate zone and then throughout the cortical wall at E17.5 and P0 (26–41%; E15.5: 26 ± 4.67%, $p = 0.00099$; E17.5: 35 ± 2.08%, $p = 9.08E\text{-}8$; P0: 41 ± 4.46%, $p = 2.48E\text{-}6$) (Figures 2A–2C and 2E–2G). Even though there was ~2-fold increased interneuron cell death at P7 (activated caspase-3, Figures S3A and S3B), P30 mice maintained ~15% (15 ± 5.43%, $p = 0.044$) more interneurons (Figures 2D and 2H). Surprisingly, while SST^+, VIP^+, NPY^+ and $reelin^+$ interneuron subtypes were increased (28–44%; SST: 32 ± 5.07%, $p = 0.001$; VIP: 44 ± 7.99%, $p = 0.014$; NPY: 34 ± 7.42%, $p = 0.0019$; reelin: 28 ± 3.01%, $p = 2.7E\text{-}5$), PV^+ interneuron density was normal (Figures 3A–3E, 3A′–3E′, and 3F–3J). MRI quantification showed that P30 cortical volume was increased 10% (10 ± 1.40%, $p = 0.0055$) (Figures S3F and S3G and Table S3). Nissl section analysis supported the MRI findings, and showed 11% increased (11 ± 3.13%, $p = 0.03$) rostral neocortical width (Figures S2A and S2B). Assessment of $NeuN^+$ (neuronal marker) cells in the P21 somatosensory cortex suggests that the enhancement in cortical volume may be the result of increased neuron numbers. In *NPAS1*$^{-/-}$ mutants, the density of $NeuN^+$ cells was increased by 11% (cortex: 11 ± 2.21%, $p = 0.0011$; layer I: 22 ± 7.34%, $p = 0.030$; layer IV: 7 ± 2.09%, $p = 0.025$; layer V: 16 ± 3.32%, $p = 0.0024$; layer VI: 13 ± 2.66%, $p = 0.0052$) (Figures S4A and S4B).

Increased Synaptic Inhibition onto Neocortical Pyramidal Neurons in *NPAS1*$^{-/-}$

To test whether the increase in cortical interneurons altered the physiology of the *NPAS1*$^{-/-}$ cortex we performed patch-clamp recordings of layer II/III somatosensory pyramidal neurons in slices from P21-30 *NPAS1*$^{-/-}$ mice and wildtype (WT) littermates (Figures 4A–4C). Compared to WT littermates, pyramidal neurons from *NPAS1*$^{-/-}$ mice showed an increase in the frequency of spontaneous IPSCs (sIPSCs) (Wildtype: 8.17 ± 1.29 Hz; *NPAS1*$^{-/-}$: 11.18 ± 1.26 Hz; $p = 0.042$). However, the amplitudes and kinetics of inhibitory events were not significantly changed (Figures 4A and 4B). To further characterize the increase in GABA-mediated synaptic inhibition, tetrodotoxin (TTX) was added to the ACSF to isolate miniature IPSCs (mIPSCs). Similar to spontaneous events, an increase in mIPSC frequencies was observed in *NPAS1*$^{-/-}$ mice (Wildtype: 6.2 ± 1.24 Hz; *NPAS1*$^{-/-}$: 8.74 ± 1.02 Hz; $p = 0.036$); amplitudes and kinetics of mIPSCs were not significantly changed (Figure 4C).

Next, we evaluated the ratio of interneuron numbers to total neuron numbers by quantifying the percentage of $NeuN^+$ cells (total neurons) that express *GAD67-GFP* in each layer of P21 somatosensory cortex (Figures S4B and S4C). At P21, all $NeuN^+$ cells were $GAD67\text{-}GFP^+$ in layer I somatosensory cortex. $NPAS1^{-/-}$ mutant mice displayed a 19% increase (19 ± 5.94%, $p = 0.025$) in $GAD67\text{-}GFP^+$ interneurons within layer I (Figure S4C). In layer II/III, the percentage of $NeuN^+$ cells that express *GAD67-GFP* was increased by 18% in $NPAS1^{-/-}$ mutants ($NPAS1^{+/+}$: 27 ± 1.13%; $NPAS1^{-/-}$: 32 ± 0.96%, $p = 0.0024$) (Figures 4D–4I). We also estimated the excitatory to inhibitory cell ratio (E/I) in each cortical layer at P21. The E/I ratio, determined as the ratio of $NeuN^+$ and $GAD67^-$ cells to $GAD67^+$ cells, was decreased by 23% in layer II/III of the $NPAS1^{-/-}$ somatosensory cortex ($NPAS1^{+/+}$: 2.74 ± 0.17; $NPAS1^{-/-}$: 2.12 ± 0.091, $p = 0.0040$) (Figure S4D). No significant change in the E/I cell ratio was found in deep cortical layers (IV, V, or VI) (Figure S4D). These findings were supported by stereological quantification of $NeuN^+$ and $GAD67^+$ cells within the cerebral cortex. The $NPAS1^{-/-}$ mutant cerebral cortex exhibited a 35% increase (35 ± 5.96%, $p = 0.0053$) in $NeuN^+$ cells and a 57% increase (57 ± 10.49%, $p = 0.0012$) in $GAD67^+$ cells at 3 months of age (Figures S4E–S4G). Cortical pyramidal cell density was unchanged in P21 $NPAS1^{-/-}$ mutants as indicated by $Cux1^+$, $Ctip2^+$, and $Tbr1^+$ immunofluorescence staining which labels layer II/III, layer V, and layer VI, respectively (Figures S4H–S4K). Thus, the enhanced level of synaptic inhibition onto layer II/III neocortical pyramidal neurons in the $NPAS1^{-/-}$ mutant was associated with an increased fraction of inhibitory neurons.

NPAS1$^{-/-}$ and *NPAS3*$^{-/-}$ Had Opposite Effects on Cortical Interneuron Numbers

$NPAS3^{-/-}$ mice display reduced proliferation and size of the adult hippocampal dentate gyrus (Pieper et al., 2005). Given that $NPAS1^{-/-}$ mutants have increased cortical volume (Figures S3F and S3G) and interneuron numbers (Figures 3A–3C, 3E, 3A′–3C′, 3E′, 3F–3H, and 3J), we hypothesized that *NPAS1* and *NPAS3* may have opposing functions on interneuron development. Therefore, we compared interneuron numbers in $NPAS1^{-/-}$, $NPAS3^{-/-}$ and $NPAS1/3^{-/-}$ P30 neocortices. While $NPAS1^{-/-}$ mutants had increased density of cortical interneurons (Figures 3A–3C, 3E, 3A′–3C′, 3E′, 3F–3H, and 3J), $NPAS3^{-/-}$ mutants had reduced density of SST^+, VIP^+, NPY^+ and $reelin^+$ interneurons (Figures 3A–3C, 3E, 3A″–C″, 3E″, 3F–3H, and 3J). Like $NPAS1^{-/-}$ mutants, there was not a change in the density of PV^+ interneurons (Figures 3D—3D″ and 3I).

MRI quantification revealed that P30 cortical volume was increased in $NPAS1^{-/-}$ mutant mice, as opposed to a 21% decrease (21 ± 1.47%, $p = 0.0039$) in $NPAS3^{-/-}$ mutants. Also, we found differential changes in P30 $NPAS1^{-/-}$ and $NPAS3^{-/-}$ mutant basal ganglia volumes by MRI. $NPAS1^{-/-}$ mutant mice displayed a 12% increase (12% ± 1.74%, $p = 0.042$) and $NPAS3^{-/-}$ mutants a 25% decrease (25% ± 2.24%, $p = 0.0087$) in basal ganglia volume (Figures S3F–S3H and Table S3).

$NPAS1/3^{-/-}$ and $NPAS3^{-/-}$ mutants had similar interneuron phenotypes (Figures 3A–E, 3A″–3E″, 3A‴–3E‴, and 3F–3J). In addition, we observed probable $NPAS1^{-/-}$, $NPAS3^{-/-}$, and $NPAS1/3^{-/-}$ mutant basal ganglia phenotypes (N=1), which include subtle cholinergic defects (*NPAS1* and *NPAS3* are expressed in the pallidum) (Figure 1 and data not shown)

(Flandin et al., 2010; Nobrega-Pereira et al., 2010). The distribution of choline acetyltransferase (ChAT)$^+$ cells around the globus pallidus (GP) was abnormal in *NPAS1/3*$^{-/-}$ and *NPAS3*$^{-/-}$ mutants. We detected increased ChAT$^+$ cells inside the GP and reduced numbers in the ventral pallidum. While parvalbumin (PV)$^+$ expression in the GP was not grossly abnormal in the mutants, the GP may be enlarged in the *NPAS1*$^{-/-}$ mutant, and smaller in the *NPAS3*$^{-/-}$ mutant. PV$^+$ interneuron numbers in the striatum and basolateral nucleus of the amygdala appeared grossly normal in all three mutant genotypes (data not shown).

NPAS1$^{-/-}$ and *NPAS3*$^{-/-}$ Ganglionic Eminences Had Opposite Proliferation and ERK-Signaling Phenotypes

Given that *NPAS1* and *NPAS3* are expressed in MGE and CGE progenitors (Figures 1A and 1B), we explored whether changes in interneuron numbers in *NPAS1*$^{-/-}$ and *NPAS3*$^{-/-}$ mutants were due to changes in proliferation using a marker of M-phase cells (phospho-histone H3, PH3). We found that *NPAS1*$^{-/-}$ mutants had a 1.6-fold increase (1.61 ± 0.13, p = 0.0007) in PH3$^+$ cells in the VZ, and a 1.3-fold increase (1.31 ± 0.039, p = 0.0033) in the SVZ of the CGE at E13.5; at E15.5 *NPAS1*$^{-/-}$ mutants had a 1.3-fold increase (VZ: 1.32 ± 0.042, p = 1.09E-5; SVZ: 1.30 ± 0.035, p = 0.022) in PH3$^+$ cells in the VZ and SVZ of the MGE (Figures 5A, 5B, 5E, 5F, 5I, and 5K). In contrast, *NPAS3*$^{-/-}$ progenitors displayed reduced proliferation in the E13.5 MGE, including a 1.3-fold decrease (1.26 ± 0.043, p = 0.010) in PH3$^+$ cells in the VZ and a 1.4-fold decrease (1.44 ± 0.031, p = 6.54E-5) in the SVZ (Figures 5Q, 5R, and 5W).

BrdU labeling analysis of E13.5 MGE and CGE progenitors, utilized to detect cells in S-phase, supported the PH3 results. 1 hour BrdU pulse-labeling showed increased proliferation in the SVZ of the *NPAS1*$^{-/-}$ mutant MGE (total number: 31 ± 1.26%, p = 0.0007; density: 48 ± 2.15%, p = 0.0004) and CGE (total number: 19 ± 3.31%, p = 0.039; density: 34 ± 5.24%, p = 0.022), while *NPAS3*$^{-/-}$ mutant mice exhibited decreased proliferation in the MGE SVZ (total number: 26 ± 2.05%, p = 0.0018; density: 21 ± 3.08%, p = 0.023) (Figures S5A–S5E). In addition, examination of proliferation in the hippocampal dentate gyrus following intraperitoneal injection of BrdU once daily for 12 days revealed a 31% increase (31 ± 7.89%, p = 0.003) in BrdU$^+$ cells in 5–10 week old *NPAS1*$^{-/-}$ mice (Figures S5F and S5G).

The *NPAS Drosophila* homolog *Trachealess* regulates FGF signaling (Ohshiro and Saigo, 1997); thus we examined activation of the MAP kinase pathway by measuring the level of phospho-ERK immunofluorescence. *NPAS1* mutants had a 1.3-fold increase (E13.5 CGE: 1.32 ± 0.043, p = 0.0016; E15.5 MGE: 1.35 ± 0.063, p = 0.00017) in phospho-ERK expression in the E13.5 CGE and E15.5 MGE, whereas *NPAS3* mutants exhibited a 1.3-fold decrease (1.26 ± 0.060, p = 0.0079) in phospho-ERK expression in the E13.5 CGE and a 1.2-fold decrease (1.17 ± 0.024, p = 0.023) in the E13.5 MGE (Figures 5C, 5D, 5G, 5H, 5J, 5L, 5O, 5P, 5S, 5T, 5V, and 5X).

NPAS1$^{-/-}$ Ganglionic Eminences Displayed Increased *Arx* Expression Which Mediated an Increase in Subpallial MAP Kinase Activity and Proliferation

We focused on identifying molecular mechanisms underlying the increased proliferation and phospho-ERK expression in the MGE and CGE of *NPAS1* mutants by ISH screening of the MGE and CGE for expression of genes that are implicated in these processes (*Arx, COUP-TFI, Cyclin D1, Cyclin D2, Dlx1, ErbB4, FGFR1, FGFR3, Lhx2, Lhx6, NPAS3, Olig1, Sp8,* and *Sprouty2*) (Figure 6 and Figure S5 and data not shown). While we did not find robust changes for most of these, including FGF-signaling components, there were some interesting changes in *Arx* and *Sp8* expression. In accordance with the increase in CGE proliferation, there was a subtle increase in $Sp8^+$ (LGE/CGE marker) migrating interneurons at E13.5 (Figure 6B) (Ma et al., 2012). We also observed a clear increase of *Arx* TF RNA at E13.5 and E15.5 in regions of the MGE and CGE where *NPAS1* is normally expressed (Figures 6A and 6C). *Arx* function is necessary for proper interneuron migration and maturation (Colombo et al., 2007; Kitamura et al., 2002; Marsh et al., 2009), as well as neocortical neuron progenitor proliferation (Friocourt et al., 2008; Kitamura et al., 2002).

To test whether NPAS1 and its co-factor, ARNT, can directly repress *Arx* expression through a known *Arx* subpallial enhancer element (Colasante et al., 2008; Visel et al., 2013), we performed luciferase assays in CGE primary cultures (Flandin et al., 2011). We found that this enhancer had two putative *NPAS1/ARNT* sites, designated A and B (Figure S7D) (Hogenesch et al., 1997). Consistent with the aforementioned phenotype, NPAS1/ARNT induced a ~2-fold repression of the *Arx* enhancer (0.58 ± 0.035, $p = 6.69E\text{-}5$). Mutation of the *Arx* enhancer at site A, but not site B, resulted in a rescue of the repression induced by NPAS1/ARNT ($p = 0.034$) (Figures 7C and 7D).

Next, to investigate whether the increase in *Arx* expression (Figures 6A and 6C) could alter subpallial development we used ultrasound to guide injection into the E13.5 CGE of a lentivirus encoding either *Arx* and *GFP*, or *GFP* alone. At E15.5, we compared the number of $PH3^+/GFP^+$ cells and observed that the *Arx*-encoding virus increased $PH3^+/GFP^+$ cells by ~2-fold (2.18 ± 0.039, $p = 0.042$) (Figures 7A and 7B and Figure S7A). We also assessed the level of phospho-ERK expression in GFP^+ regions of the CGE ventricular zone and found that *Arx* overexpression increased phospho-ERK expression by 1.4-fold (1.39 ± 0.12, $p = 0.046$) (Figures S7B and S7C). These findings provide evidence that NPAS1 repression of *Arx* can regulate CGE proliferation and MAP kinase activity.

Non-Synonymous Mutations in *NPAS1 and NPAS3* Are Found in Humans with ASD

NPAS3 mutations are observed in patients with schizophrenia (Kamnasaran et al., 2003; Macintyre et al., 2010). Given that autism spectrum disorders (ASD) and schizophrenia share some genetic risk factors (Murdoch and State, 2013) and, like *NPAS1* mutant mice, enlarged brain size is frequent in ASD children (Butler et al., 2005; Hazlett et al., 2011), we screened 947 ASD probands for mutations in *NPAS1* and *NPAS3* exons, introns, and 5′ and 3′ untranslated regions, and found 10 non-synonymous variants in *NPAS1* and seven in *NPAS3* (See the Supplemental Text). We assayed 13 of those in 190 control subjects (unscreened for autism) and found that five of seven in *NPAS1* and all six in *NPAS3* were absent in the controls. Although the data lacks statistical power, and does not

unambiguously implicate these variants in genetic susceptibility to ASD, these results support the possibility that *NPAS1* and *NPAS3* mutations are related to ASD risk.

Discussion

NPAS1$^{-/-}$ mice had increased numbers of neocortical interneurons, whereas *NPAS3*$^{-/-}$ mice have fewer interneurons (Figures 3A–3C, 3E, 3A′–3C′, 3E′, 3A″–3C″, 3E″, 3F–3H, and 3J). These changes in interneuron numbers were associated with altered ERK signaling and cell proliferation within the MGE and CGE of *NPAS1*$^{-/-}$ and *NPAS3*$^{-/-}$ mutants (Figure 5). In addition, the increased numbers of neocortical interneurons in *NPAS1*$^{-/-}$ mice resulted in enhanced synaptic inhibition onto neocortical pyramidal neurons in layer II/III of the somatosensory cortex (Figures 4A–4C). We focused on how *NPAS1* regulates this process in the MGE and CGE, and found that *NPAS1*$^{-/-}$ mutants had increased *Arx* expression in these embryonic progenitor zones (Figures 6A and 6C). Using *in utero* transduction of *Arx* into the CGE, we showed that increased *Arx* expression was sufficient to increase subpallial proliferation and MAP kinase activity (Figures 7A and 7B and Figures S7B and S7C). We also demonstrated that NPAS1 could directly repress a *bone fide Arx* subpallial enhancer (Figures 7C and 7D and Figure S7D) (Colasante et al., 2008).

Our results provide novel insights into mechanisms that control the number of specific subtypes of cortical inhibitory neurons, showing that homologous TF-encoding genes *NPAS1* and *NPAS3* have opposing functions in regulating the numbers of SST^+, and VIP^+ interneurons (Figures 3A—3A″, 3E–3E″, 3F, and 3J). Thus, we have provided evidence for a cell autonomous mechanism that controls interneuron numbers, a process proposed to exist based on results from the MGE-transplantation assay (Southwell et al., 2012).

NPAS1 and *NPAS3* Regulate the Proliferation of Ganglionic Eminence Progenitors

Proliferation and ERK signaling in progenitor domains of the MGE and CGE were increased and decreased in *NPAS1*$^{-/-}$ and *NPAS3*$^{-/-}$ mice, respectively (Figure 5). Vertebrate *NPAS* function in embryonic neural precursors may be related to the function of *Trachealess*, the *NPAS Drosophila* homolog. *Trachealess* promotes FGF-signaling by increasing expression of the FGF receptor (Ohshiro and Saigo, 1997). This program is evolutionary conserved based on the observation that *NPAS3*$^{-/-}$ mice have reduced *FGFR1* expression in the adult hippocampus (Pieper et al., 2005). However, *NPAS3*$^{-/-}$ mutant mice did not show this phenotype in the prenatal telencephalon (data not shown). Also, *NPAS1*$^{-/-}$ mutants did not exhibit decreased *FGFR1* expression in the adult hippocampus (Pieper et al., 2005), or in the prenatal telencephalon (Figure S6C). Thus, there is no evidence that changes in phospho-ERK levels, in the subpallium of *NPAS1*$^{-/-}$ and *NPAS3*$^{-/-}$ mutants (Figures 5C, 5D, 5G, 5H, 5J, 5L, 5O, 5P, 5S, 5T, 5V, and 5X), is related to altered FGF-signaling.

Our study reveals new insights into *NPAS1* regulation of cell proliferation. Here, we have found that the increase in proliferation and MAPK signaling in *NPAS1*$^{-/-}$ mutant CGE and MGE progenitors was associated with increased *Arx* expression. Previous studies of *Arx* mutant mice show that lack of this TF resulted in reduced cortical proliferation (Friocourt et al., 2008; Kitamura et al., 2002). We demonstrated that increased *Arx* expression was sufficient to enhance subpallial proliferation and MAP kinase activity, using *in utero*

transduction of *Arx* into the CGE (Figures 7A and 7B and Figures S7B and S7C). Furthermore, we showed that NPAS1 could directly inhibit a *bone fide Arx* subpallial enhancer (Figures 7C and 7D and Figure S7D) (Colasante et al., 2008).

Given that *NPAS1* and *NPAS3* have opposite effects on proliferation, an imbalance of either *NPAS1* or *NPAS3* expression and/or function could potentially be compensated by changes in the expression of the other gene. However, we did not observe changes of *NPAS3* expression in the *NPAS1*$^{-/-}$ E13.5 and P0 forebrain (data not shown).

NPAS1 and *NPAS3* Modified the Production of Specific Subtypes of Cortical Interneurons

The increase in *Arx* and phospho-ERK expression and the increase in proliferation in the MGE and CGE of *NPAS1*$^{-/-}$ mutants were associated with an increase in subpallially-derived cortical interneurons (Figure 2). As a result, *NPAS1* mutants had excessive SST^{+} and VIP^{+} interneurons, products of the MGE and CGE, respectively (Figures 3A, 3A′, 3E, 3E′, 3F, and 3J) (Rudy et al., 2011). In contrast, decreased phospho-ERK expression and cell proliferation in the MGE and CGE of *NPAS3*$^{-/-}$ mutant mice resulted in reduced numbers of SST^{+} and VIP^{+} interneurons (Figures 3A, 3A″, 3E, 3E″, 3F, and 3J).

Both *NPAS1* and *NPAS3* mutants had a normal density of PV^{+} interneurons (Figures 3D—3D″, and 3I). PV and SST are MGE-derived (Rudy et al., 2011). *NPAS1*, along with *NPAS3*, *COUP-TFI, Dlx1* and *SatB1* (Cobos et al., 2005; Denaxa et al., 2012; Lodato et al., 2011) define a set of TFs that differentially regulate the numbers of interneurons that express PV and SST (Figures 3D—3D″, 3E–3E″, 3I, and 3J). At least one PV^{+} subtype, the Chandelier neuron, is generated late in gestation (Inan et al., 2012; Taniguchi et al., 2013); perhaps *NPAS1* and *NPAS3* regulation of MGE proliferation is time-dependent, and thus preferentially affects early-born SST^{+} interneurons. Based on the embryonic phenotypes of *NPAS1*$^{-/-}$ and *NPAS3*$^{-/-}$ mutants, we propose that NPAS1 and NPAS3 control the SST/PV ratio via their functions in MGE progenitor cells. Future studies are needed to examine the roles of NPAS1 and NPAS3 in regulating interneurons via their expression in maturing and mature interneurons (Figure 1C).

The significance of transcriptional repression in the regulation of cortical interneuron number is becoming apparent. A recent study demonstrates that Olig1 inhibits the generation of GABAergic interneurons produced in the MGE by repression of *Dlx* expression through the *Dlx1/2 I12b* intergenic enhancer (Silbereis et al., 2014). Likewise, NPAS1 inhibits the generation of cortical interneurons by repression of Arx expression through the subpallial *Arx* enhancer, which mediates CGE progenitor cell proliferation (Figure 7) (Colasante et al., 2008).

NPAS1 Function in Interneuron Generation Controls Cortical Excitation/Inhibition

NPAS1$^{-/-}$ mutant mice display increased numbers of GAD67-GFP^{+} interneurons in layer I (Figure S4C). It is likely that an excess of GABAergic neurons in layer I would have an effect on the inhibitory tone of pyramidal cell dendrites within this layer. *NPAS1* mutants also exhibit excessive SST^{+} and VIP^{+} interneurons. VIP^{+} interneurons are enriched in layers II/III (Kawaguchi and Kubota, 1997; Miyoshi et al., 2010), and form synapses with

pyramidal cell somata and dendrites (Kawaguchi and Kubota, 1996) and other interneurons (Acsády et al., 1996; Dávid et al., 2007; Hajos et al., 1996). Thus, with an increase in both SST^+ and VIP^+ interneurons, it is difficult to deduce the net physiological effect *a priori*. We found that *NPAS1* mutants had enhanced cortical inhibition in layer II/III of the somatosensory cortex (Figure 4), implying that the increase in interneurons resulted in a net increase in inhibition in superficial cortical layers. The enhanced cortical inhibition in layer II/III somatosensory cortex of $NPAS1^{-/-}$ mutants suggests a decreased E/I ratio in layer II/III somatosensory cortex. This is supported by estimation of the cellular E/I ratio within this cortical region of $NPAS1^{-/-}$ mutant mice (Figure S4D). While increased cortical inhibition is likely to reduce noise in the cortex, and it could be protective for epilepsy, it may be detrimental to cortical function by dampening cortical signals and thereby predispose to neuropsychiatric disorders.

NPAS1 and *NPAS3* in Human Neuropsychiatric Disorders

Our examination of NPAS1 and NPAS3 functions in mice provides novel mechanistic insights into human neuropsychiatric disorders. $NPAS3^{-/-}$ mutant mice display behavioral and neuroanatomical deficits associated with human schizophrenia (Erbel-Sieler et al., 2004) and *NPAS3* mutations are observed in patients with schizophrenia (Kamnasaran et al., 2003; Macintyre et al., 2010). Furthermore, *NPAS1* mutant mice exhibit an increase in brain size (Figures S3D–S3G), similar to the enlargement seen in some children with autism spectrum disorders (ASD) (Butler et al., 2005; Hazlett et al., 2011). Notably, we have found sporadic non-synonymous mutations in *NPAS1* and *NPAS3* in individuals with ASD, which suggests that *NPAS1* and *NPAS3* mutations may be associated with ASD risk. However, our analyses lack the statistical power to conclude that these alleles contribute to ASD. Nonetheless, these data, and the experimental analyses of the mouse mutants, strongly suggest that further genetic analyses of *NPAS1* and *NPAS3* are warranted in human neuropsychiatric disorders.

Experimental Procedures

Mice

$NPAS1^{+/-}$ and $NPAS3^{+/-}$ mice were obtained from Steven McKnight (University of Texas Southwestern Medical Center) and genotyped as described by Erbel-Sieler and colleagues (Erbel-Sieler et al., 2004). $NPAS1^{+/-}$ mice were maintained in a C57BL/6J strain background. $NPAS1^{+/-}$; $NPAS3^{+/-}$ females mated to $NPAS1^{+/-}$; $NPAS3^{+/-}$ males also produced C57Bl/6J strain litters. $NPAS3^{-/-}$ mutant mice obtained from this cross were utilized for BrdU analysis of the ganglionic eminences, assessment of cortical layer-specific markers, and in the examination of interneuron markers in the P30 somatosensory cortex. However, due to increased mortality of $NPAS3^{-/-}$ mutants maintained on a C57BL/6J strain background, subsequent experiments were performed with $NPAS3^{-/-}$ mutant mice maintained on a CD-1 strain background. These experiments include assessment of apoptosis within the somatosensory cortex, examination of PH3 and phospho-ERK expression in the ganglionic eminences, and MRI analysis.

The *Lhx6-GFP* BAC transgenic mouse line was obtained from The Gene Expression Nervous System Atlas Project (GENSAT) at The Rockefeller University (New York, NY).

GAD67-GFP mice were genotyped as described by Tamamaki and colleagues (Tamamaki et al., 2003). As a note on nomenclature, experimental samples designated as *NPAS1*$^{+/+}$ indicates that the *NPAS1* allele is unaltered; however data from these mice are not referred to as wildtype because they have either the *Lhx6-GFP* or *GAD67-GFP* alleles. CD-1 wildtype mice were obtained from Charles River Laboratories. Wildtype littermate mice were used as controls for all experiments. For staging of embryos, midday of the vaginal plug was calculated as embryonic day 0.5 (E0.5). Mouse colonies were maintained at the University of California, San Francisco and University of Texas Southwestern Medical Center, in accordance with National Institutes of Health, UCSF, and UT Southwestern guidelines.

Histology

See the Supplemental Experimental Procedures for details on immunohistochemistry, *in situ* hybridization, BrdU labeling, and Nissl stain analysis.

Magnetic Resonance Imaging (MRI)

P30 4% PFA-fixed brains were washed twice in 20 mL PBS for a total of 24 hours and imaged in Fluorinert FC-40 (Sigma Aldrich) for null background signal. The imaging was done on an 600 MHz NMR spectrometer (Agilent Technologies Inc.) with imaging gradients and the following parameters: 3D gradient echo, TE/TR 15/75 ms, 8 averages, field of view (FOV) 12.8 mm isotropic, resolution of 50 μm × 50 μm × 100 μm, and a total scan time of 5.5 hours. The acquired images were converted on the Varian console to the DICOM format and reformatted into the same orientation as the histology sections using OsiriX, an open source image viewer. Volumetric measurements were made using custom-built software in MATLAB. Cortical and basal ganglia volumes were statistically analyzed in three mice of each genotype. Results are presented as mean ± SEM. Statistical differences between experimental groups were assessed with the Student's *t*-test using SPSS 15 software (IBM). See Table S3 in the Supplemental Experimental Procedures for details on cortical and basal ganglia volumes in control, *NPAS1*$^{-/-}$, and *NPAS3*$^{-/-}$ mutants.

Electrophysiology

Coronal brain slices (300 μm) were prepared from P21-30 wildtype and *NPAS1*$^{-/-}$ mice. Slices were submerged in the recording chamber and continuously perfused with oxygenated ACSF (32–34°C) containing (in mM): 124 NaCl, 3 KCl, 1.25 NaH_2PO_4-H_2O, $2MgSO_4$-$7H_2O$, 26 $NaHCO_3$, 10 dextrose, and 2 $CaCl_2$ (pH 7.2–7.4, 300–305 mOsm/kg). Whole-cell patch-clamp recordings from layer II/III pyramidal cells in somatosensory neocortex were performed at 40X using an upright, fixed-stage microscope (Olympus BX50WI) equipped with infrared, differential interference contrast (IR-DIC). Patch pipettes (2–4 MΩ) were filled with an internal solution, containing (in mM): 140 CsCl, 1 $MgCl_2$, 10 HEPES, 11 EGTA, 2 NaATP, 0.5 Na_2GTP and 1.25 QX-314, pH 7.28. Recordings were obtained with an Axopatch 1D amplifier, filtered at 5 kHz, and recorded to pClamp 10.2 software (Clampfit, Axon Instruments). Spontaneous (s) and miniature (m) IPSCs were examined at a holding potential of −70 mV. GABAergic currents were isolated by adding 1mM kynurenic acid to the ACSF to block glutamate receptors, and tetrodotoxin (TTX,

2μM) was added to isolate mIPSCs. Series resistance was typically <15 MΩ and was monitored throughout the recordings. Data were only used for analysis if the series resistance remained <20 MΩ and changed by ≤20% during the recordings. Data analysis was performed using pClamp 10.2 (Clampfit, Axon Instruments), MiniAnalysis 6.0 (Synaptosoft), Microsoft excel, and Sigmaplot 12.3 programs. Events characterized by a typical fast rising phase and exponential decay phase were manually detected using MiniAnalysis. A 2 min sample recording per cell was used for measuring IPSC frequency, amplitude, 10–90% rise time, and decay time constant. Kinetic analysis of the IPSCs was performed with a single-exponential function. The threshold for event detection was currents with amplitudes greater than three times the root mean square (RMS) noise level. Spontaneous IPSC measurements were recorded from 18 wildtype and 20 *NPAS1*$^{-/-}$ pyramidal cells. Miniature IPSC measurements were recorded from 14 wildtype and 16 *NPAS1*$^{-/-}$ pyramidal cells. Seven wildtype and nine *NPAS1*$^{-/-}$ animals were used for sIPSC and mIPSC measurements. Results are expressed as mean ± SEM. Statistical differences between experimental groups were assessed with the Mann–Whitney *U* test using SigmaPlot 12.3 software (SYSTAT).

Primary Cell Culture and Luciferase Assays

CGE tissue was dissected from E12.5 WT embryos and mechanically dissociated with a P1000 pipette tip. 200,000 cells were seeded into tissue culture dishes precoated with poly-L-lysine 10 μg/ml, Sigma) then laminin (5 μg/ml, Sigma), and grown in N5 media (DMEM-F-12 with glutamax, N2 supplement, 35 μg/ml bovine pituitary extract, 20 ng/ml bFGF, and 20 ng/ml EGF) as previously described for MGE cells (Flandin et al., 2011).

CGE primary cultures were transfected using Fugene® 6 (Promega) with DNA expression vectors and reporters comprising four conditions: 1) empty firefly-luciferase reporter (PGL4.23) and a control DNA expression vector only expressing GFP (CMV-GFP), 2) empty PGL4.23 and CMV-NPAS1, 3) Arx enhancer (UAS3-PGL4.23) luciferase reporter and CMV-GFP, and 4) UAS3-PGL4.23 and CMV-NPAS1. All conditions also included the same amounts of CMV-ARNT (NPAS co-factor) and Renilla-luciferase (normalization control). Cell lysates were collected at two days post-transfection and procedures were performed according to the manufacturer's protocol (Promega, dual luciferase assay system). Enhancer activity for each condition was determined from three independent experiments, each performed in triplicate. Results were calculated as mean ± SEM and presented as fold change relative to the basal condition containing CMV-GFP and the PGL4.23 empty luciferase reporter vector. Statistical differences between experimental groups were determined with the Student's *t*-test using SPSS 15 software (IBM). See the Supplemental Experimental Procedures for details on expression and luciferase reporter vectors.

Virus Production and *In Utero* Injection

HEK293T cells grown in DMEM H21 with 10% FBS were transfected with four plasmids to generate lentivirus particles, (pVSV-g, pRSVr, pMDLg-pRRE and the lentiviral vector). Cells were transfected at ~70% confluency and media was completely replaced four hours after transfection, then cultured for four days before harvesting. On day four of culture, all

the media (~35 mls) was collected and filtered through a 0.45 low protein binding membrane to remove cells and large debris. The filtered media was pooled and ultracentrifuged at 100,000 × g for 2.5 hours at 4°C. After the ultracentrifuge step, supernatant was removed and the pellet was resuspended overnight in sterile PBS then stored at −80°C until use. For infection, recipient pregnant females (E13.5) were anesthetized with isoflurane, their uterine horns exposed, and mounted under an ultrasound microscope (Vevo 770, VisualSonics). A beveled glass micropipette (~50 μm diameter) was front loaded with CMV-GFP or CMV-GFP-T2a-Arx lentivirus and inserted into the ventricular zone of the CGE under real-time ultrasound guidance imaging. ~1 μl of solution was injected into the ventricular zone of the CGE. Three successfully injected animals were analyzed two days later (E15.5) for each experimental condition. Image analysis of CMV-GFP$^+$/PH3$^+$, CMV-GFP$^+$/phospho-ERK$^+$, CMV-GFP-T2a-Arx$^+$/PH3$^+$ or CMV-GFP-T2a-Arx$^+$/phospho-ERK$^+$ co-expression was performed on images acquired on a confocal microscope (LSM 510 META NLO, Carl Zeiss International) with a 20X objective. The percentage of CMV-GFP$^+$ or CMV-GFP-T2a-Arx$^+$ that express PH3 was calculated in a 10,000 μm^2 area of the CGE ventricular zone. Results are presented as mean ± SEM. Statistical differences between experimental groups were assessed with the chi-squared test using SPSS 15 software (IBM). Phospho-ERK expression levels were measured in GFP$^+$ regions of the CGE ventricular zone with the aid of Adobe Photoshop CS4 software. Expression levels were determined as a ratio of the integrated density of phospho-ERK$^+$ CGE ventricular zone cells in a 4,000 μm^2 area to the integrated density of phospho-ERK$^+$ cortical ventricular zone cells in a 4,000 μm^2 area. Integrated density is equal to the sum of the pixel values in a selected area. Results were calculated as mean ± SEM and presented as fold change relative to control. Statistical differences between experimental groups were determined with the Student's *t*-test using SPSS 15 software (IBM). See the Supplemental Experimental Procedures for details on lentiviral vectors.

Human DNA Sequencing

See the Supplemental Experimental Procedures for details on human DNA sequencing.

Supplementary Material

Refer to Web version on PubMed Central for supplementary material.

Acknowledgments

We are grateful to S. McKnight and his lab at University of Texas Southwestern Medical Center for the generous gift of NPAS1 and NPAS3 antibodies, the *NPAS1*$^{+/-}$ and *NPAS3*$^{+/-}$ mice, the NPAS1 in situ hybridization construct (J. Walker), and the CMV-ARNT and CMV-NPAS1 mammalian expression vectors (L. Wu). We acknowledge the Autism Genetic Resource Exchange (AGRE) and Simons Foundation Autism Research Initiative (SFARI) for ASD genomic DNA samples, and SFARI as well for phenotypic data made available on SFARI Base. We also wish to thank all the families who donated samples and the principal investigators involved in their collection (A. Beaudet, R. Bernier, J. Constantino, E. Cook, E. Fombonne, D. Geschwind, D. Grice, A. Klin, D. Ledbetter, C. Lord, C. Martin, D. Martin, R. Maxim, J. Miles, O. Ousley, B. Peterson, J. Piggot, C. Saulnier, M. State, W. Stone, J. Sutcliffe, C. Walsh, E. Wijsman). Approved researchers can obtain the Simons Simplex Collection (SSC) population dataset by applying at https://base.sfari.org. This work was supported by research grants to JLRR (Simons Foundation, Nina Ireland, Althea Foundation, NIMH R37 MH049428, Weston Havens Foundation), to AS (NIMHT32 MH089920), to SCB (R01NS071785), to RFH (F32NS077747) to DX (R01EB009756), to SPH (Jaffe Family Foundation), and to AAP and Steven L. McKnight (NIMH 5-RO1-

MH087986). This work was also funded in part by an unrestricted endowment provided to Steven L. McKnight by an anonymous donor used as support for JW.

References

Acsády L, Arabadzisz D, Freund TF. Correlated morphological and neurochemical features identify different subsets of vasoactive intestinal polypeptide-immunoreactive interneurons in rat hippocampus. Neuroscience. 1996; 73:299–315. [PubMed: 8783251]

Azim E, Jabaudon D, Fame RM, Macklis JD. SOX6 controls dorsal progenitor identity and interneuron diversity during neocortical development. Nat Neurosci. 2009; 12:1238–1247. [PubMed: 19657336]

Batista-Brito R, Machold R, Klein C, Fishell G. Gene expression in cortical interneuron precursors is prescient of their mature function. Cereb Cortex. 2008; 18:2306–2317. [PubMed: 18250082]

Batista-Brito R, Rossignol E, Hjerling-Leffler J, Denaxa M, Wegner M, Lefebvre V, Pachnis V, Fishell G. The cell-intrinsic requirement of Sox6 for cortical interneuron development. Neuron. 2009; 63:466–481. [PubMed: 19709629]

Butler MG, Dasouki MJ, Zhou XP, Talebizadeh Z, Brown M, Takahashi TN, Miles JH, Wang CH, Stratton R, Pilarski R, Eng C. Subset of individuals with autism spectrum disorders and extreme macrocephaly associated with germline PTEN tumour suppressor gene mutations. J Med Genet. 2005; 42:318–321. [PubMed: 15805158]

Cobos I, Calcagnotto ME, Vilaythong AJ, Thwin MT, Noebels JL, Baraban SC, Rubenstein JLR. Mice lacking Dlx1 show subtype-specific loss of interneurons, reduced inhibition and epilepsy. Nat Neurosci. 2005; 8:1059–1068. [PubMed: 16007083]

Colasante G, Collombat P, Raimondi V, Bonanomi D, Ferrai C, Maira M, Yoshikawa K, Mansouri A, Valtorta F, Rubenstein JL, Broccoli V. Arx is a direct target of Dlx2 and thereby contributes to the tangential migration of GABAergic interneurons. J Neurosci. 2008; 28:10674–10686. [PubMed: 18923043]

Colombo E, Collombat P, Colasante G, Bianchi M, Long J, Mansouri A, Rubenstein JL, Broccoli V. Inactivation of Arx, the murine ortholog of the X-linked lissencephaly with ambiguous genitalia gene, leads to severe disorganization of the ventral telencephalon with impaired neuronal migration and differentiation. J Neurosci. 2007; 27:4786–4798. [PubMed: 17460091]

Courchesne E, Pierce K, Schumann CM, Redcay E, Buckwalter JA, Kennedy DP, Morgan J. Mapping early brain development in autism. Neuron. 2007; 56:399–413. [PubMed: 17964254]

Dávid C, Schleicher A, Zuschratter W, Staiger JF. The innervation of parvalbumin-containing interneurons by VIP-immunopositive interneurons in the primary somatosensory cortex of the adult rat. Eur J Neurosci. 2007; 25:2329–2340. [PubMed: 17445231]

Denaxa M, Kalaitzidou M, Garefalaki A, Achimastou A, Lasrado R, Maes T, Pachnis V. Maturation-promoting activity of SATB1 in MGE-derived cortical interneurons. Cell Rep. 2012; 2:1351–1362. [PubMed: 23142661]

Erbel-Sieler C, Dudley C, Zhou Y, Wu X, Estill SJ, Han T, Diaz-Arrastia R, Brunskill EW, Potter SS, McKnight SL. Behavioral and regulatory abnormalities in mice deficient in the NPAS1 and NPAS3 transcription factors. Proc Natl Acad Sci U S A. 2004; 101:13648–13653. [PubMed: 15347806]

Flandin P, Kimura S, Rubenstein JL. The progenitor zone of the ventral medial ganglionic eminence requires Nkx2-1 to generate most of the globus pallidus but few neocortical interneurons. J Neurosci. 2010; 30:2812–2823. [PubMed: 20181579]

Flandin P, Zhao Y, Vogt D, Jeong J, Long J, Potter G, Westphal H, Rubenstein JL. Lhx6 and Lhx8 coordinately induce neuronal expression of Shh that controls the generation of interneuron progenitors. Neuron. 2011; 70:939–950. [PubMed: 21658586]

Friocourt G, Kanatani S, Tabata H, Yozu M, Takahashi T, Antypa M, Raguenes O, Chelly J, Ferec C, Nakajima K, Parnavelas JG. Cell-autonomous roles of ARX in cell proliferation and neuronal migration during corticogenesis. J Neurosci. 2008; 28:5794–5805. [PubMed: 18509041]

Gelman, DM.; Marin, O.; Rubenstein, JLR. The Generation of Cortical Interneurons. In: Noebels, JL.; Avoli, M.; Rogawski, MA.; Olsen, RW.; Delgado-Escueta, AV., editors. Jasper's Basic

Mechanisms of the Epilepsies. Bethesda, MD: National Center for Biotechnology Information; 2012.

Gripp KW, Zand DJ, Demmer L, Anderson CE, Dobyns WB, Zackai EH, Denenberg E, Jenny K, Stabley DL, Sol-Church K. Expanding the SHOC2 mutation associated phenotype of noonan syndrome with loose anagen hair: Structural brain anomalies and myelofibrosis. Am J Med Genet A. 2013:36098.

Hajos N, Acsady L, Freund TF. Target selectivity and neurochemical characteristics of VIP-immunoreactive interneurons in the rat dentate gyrus. Eur J Neurosci. 1996; 8:1415–1431. [PubMed: 8758949]

Hazlett HC, Poe MD, Gerig G, Styner M, Chappell C, Smith RG, Vachet C, Piven J. Early brain overgrowth in autism associated with an increase in cortical surface area before age 2 years. Arch Gen Psychiatry. 2011; 68:467–476. [PubMed: 21536976]

Hogenesch JB, Chan WK, Jackiw VH, Brown RC, Gu YZ, Pray-Grant M, Perdew GH, Bradfield CA. Characterization of a subset of the basic-helix-loop-helix-PAS superfamily that interacts with components of the dioxin signaling pathway. J Biol Chem. 1997; 272:8581–8593. [PubMed: 9079689]

Inan M, Welagen J, Anderson SA. Spatial and temporal bias in the mitotic origins of somatostatin- and parvalbumin-expressing interneuron subgroups and the chandelier subtype in the medial ganglionic eminence. Cereb Cortex. 2012; 22:820–827. [PubMed: 21693785]

Kamnasaran D, Muir WJ, Ferguson-Smith MA, Cox DW. Disruption of the neuronal PAS3 gene in a family affected with schizophrenia. J Med Genet. 2003; 40:325–332. [PubMed: 12746393]

Kawaguchi Y, Kubota Y. Physiological and morphological identification of somatostatin- or vasoactive intestinal polypeptide-containing cells among GABAergic cell subtypes in rat frontal cortex. J Neurosci. 1996; 16:2701–2715. [PubMed: 8786446]

Kawaguchi Y, Kubota Y. GABAergic cell subtypes and their synaptic connections in rat frontal cortex. Cereb Cortex. 1997; 7:476–486. [PubMed: 9276173]

Kitamura K, Yanazawa M, Sugiyama N, Miura H, Iizuka-Kogo A, Kusaka M, Omichi K, Suzuki R, Kato-Fukui Y, Kamiirisa K, et al. Mutation of ARX causes abnormal development of forebrain and testes in mice and X-linked lissencephaly with abnormal genitalia in humans. Nat Genet. 2002; 32:359–369. [PubMed: 12379852]

Kwan KY, Sestan N, Anton ES. Transcriptional co-regulation of neuronal migration and laminar identity in the neocortex. Development. 2012; 139:1535–1546. [PubMed: 22492350]

Le Magueresse C, Monyer H. GABAergic interneurons shape the functional maturation of the cortex. Neuron. 2013; 77:388–405. [PubMed: 23395369]

Lewis DA, Curley AA, Glausier JR, Volk DW. Cortical parvalbumin interneurons and cognitive dysfunction in schizophrenia. Trends Neurosci. 2012; 35:57–67. [PubMed: 22154068]

Liodis P, Denaxa M, Grigoriou M, Akufo-Addo C, Yanagawa Y, Pachnis V. Lhx6 activity is required for the normal migration and specification of cortical interneuron subtypes. J Neurosci. 2007; 27:3078–3089. [PubMed: 17376969]

Lodato S, Tomassy GS, De Leonibus E, Uzcategui YG, Andolfi G, Armentano M, Touzot A, Gaztelu JM, Arlotta P, Menendez de la Prida L, Studer M. Loss of COUP-TFI alters the balance between caudal ganglionic eminence- and medial ganglionic eminence-derived cortical interneurons and results in resistance to epilepsy. J Neurosci. 2011; 31:4650–4662. [PubMed: 21430164]

Ma T, Zhang Q, Cai Y, You Y, Rubenstein JL, Yang Z. A subpopulation of dorsal lateral/caudal ganglionic eminence-derived neocortical interneurons expresses the transcription factor Sp8. Cereb Cortex. 2012; 22:2120–2130. [PubMed: 22021915]

Macintyre G, Alford T, Xiong L, Rouleau GA, Tibbo PG, Cox DW. Association of NPAS3 exonic variation with schizophrenia. Schizophr Res. 2010; 120:143–149. [PubMed: 20466522]

Marin O. Interneuron dysfunction in psychiatric disorders. Nat Rev Neurosci. 2012; 13:107–120. [PubMed: 22251963]

Marin O. Cellular and molecular mechanisms controlling the migration of neocortical interneurons. Eur J Neurosci. 2013; 38:2019–2029. [PubMed: 23651101]

Marsh E, Fulp C, Gomez E, Nasrallah I, Minarcik J, Sudi J, Christian SL, Mancini G, Labosky P, Dobyns W, et al. Targeted loss of Arx results in a developmental epilepsy mouse model and

recapitulates the human phenotype in heterozygous females. Brain. 2009; 132:1563–1576. [PubMed: 19439424]

Miyoshi G, Hjerling-Leffler J, Karayannis T, Sousa VH, Butt SJ, Battiste J, Johnson JE, Machold RP, Fishell G. Genetic fate mapping reveals that the caudal ganglionic eminence produces a large and diverse population of superficial cortical interneurons. J Neurosci. 2010; 30:1582–1594. [PubMed: 20130169]

Murdoch JD, State MW. Recent developments in the genetics of autism spectrum disorders. Curr Opin Genet Dev. 2013; 23:310–315. [PubMed: 23537858]

Nobrega-Pereira S, Gelman D, Bartolini G, Pla R, Pierani A, Marin O. Origin and molecular specification of globus pallidus neurons. J Neurosci. 2010; 30:2824–2834. [PubMed: 20181580]

Ohshiro T, Saigo K. Transcriptional regulation of breathless FGF receptor gene by binding of TRACHEALESS/dARNT heterodimers to three central midline elements in Drosophila developing trachea. Development. 1997; 124:3975–3986. [PubMed: 9374395]

Pieper AA, Wu X, Han TW, Estill SJ, Dang Q, Wu LC, Reece-Fincanon S, Dudley CA, Richardson JA, Brat DJ, McKnight SL. The neuronal PAS domain protein 3 transcription factor controls FGF-mediated adult hippocampal neurogenesis in mice. Proc Natl Acad Sci U S A. 2005; 102:14052–14057. [PubMed: 16172381]

Poduri A, Evrony GD, Cai X, Elhosary PC, Beroukhim R, Lehtinen MK, Hills LB, Heinzen EL, Hill A, Hill RS, et al. Somatic activation of AKT3 causes hemispheric developmental brain malformations. Neuron. 2012; 74:41–48. [PubMed: 22500628]

Riviere JB, Mirzaa GM, O'Roak BJ, Beddaoui M, Alcantara D, Conway RL, St-Onge J, Schwartzentruber JA, Gripp KW, Nikkel SM, et al. De novo germline and postzygotic mutations in AKT3, PIK3R2 and PIK3CA cause a spectrum of related megalencephaly syndromes. Nat Genet. 2012; 44:934–940. [PubMed: 22729224]

Rubenstein JL, Merzenich MM. Model of autism: increased ratio of excitation/inhibition in key neural systems. Genes Brain Behav. 2003; 2:255–267. [PubMed: 14606691]

Rudy B, Fishell G, Lee S, Hjerling-Leffler J. Three groups of interneurons account for nearly 100% of neocortical GABAergic neurons. Dev Neurobiol. 2011; 71:45–61. [PubMed: 21154909]

Silbereis JC, Nobuta H, Tsai HH, Heine VM, McKinsey GL, Meijer DH, Howard MA, Petryniak MA, Potter GB, Alberta JA, et al. Olig1 function is required to repress Dlx1/2 and interneuron production in mammalian brain. Neuron. 2014; 81:574–587. [PubMed: 24507192]

Southwell DG, Paredes MF, Galvao RP, Jones DL, Froemke RC, Sebe JY, Alfaro-Cervello C, Tang Y, Garcia-Verdugo JM, Rubenstein JL, et al. Intrinsically determined cell death of developing cortical interneurons. Nature. 2012; 491:109–113. [PubMed: 23041929]

Striano P, Zara F. Genetics: mutations in mTOR pathway linked to megalencephaly syndromes. Nat Rev Neurol. 2012; 8:542–544. [PubMed: 22907262]

Sussel L, Marin O, Kimura S, Rubenstein JL. Loss of Nkx2.1 homeobox gene function results in a ventral to dorsal molecular respecification within the basal telencephalon: evidence for a transformation of the pallidum into the striatum. Development. 1999; 126:3359–3370. [PubMed: 10393115]

Tamamaki N, Yanagawa Y, Tomioka R, Miyazaki J, Obata K, Kaneko T. Green fluorescent protein expression and colocalization with calretinin, parvalbumin, and somatostatin in the GAD67-GFP knock-in mouse. J Comp Neurol. 2003; 467:60–79. [PubMed: 14574680]

Taniguchi H, Lu J, Huang ZJ. The spatial and temporal origin of chandelier cells in mouse neocortex. Science. 2013; 339:70–74. [PubMed: 23180771]

Visel A, Taher L, Girgis H, May D, Golonzhka O, Hoch RV, McKinsey GL, Pattabiraman K, Silberberg SN, Blow MJ, et al. A high-resolution enhancer atlas of the developing telencephalon. Cell. 2013; 152:895–908. [PubMed: 23375746]

Yizhar O, Fenno LE, Prigge M, Schneider F, Davidson TJ, O'Shea DJ, Sohal VS, Goshen I, Finkelstein J, Paz JT, et al. Neocortical excitation/inhibition balance in information processing and social dysfunction. Nature. 2011; 477:171–178. [PubMed: 21796121]

Zhao Y, Flandin P, Long JE, Cuesta M Dela, Westphal H, Rubenstein JLR. Distinct molecular pathways for development of telencephalic interneuron subtypes revealed through analysis of Lhx6 mutants. J Comp Neurol. 2008; 510:79–99. [PubMed: 18613121]

Zhou YD, Barnard M, Tian H, Li X, Ring HZ, Francke U, Shelton J, Richardson J, Russell DW, McKnight SL. Molecular characterization of two mammalian bHLH-PAS domain proteins selectively expressed in the central nervous system. Proc Natl Acad Sci U S A. 1997; 94:713–718. [PubMed: 9012850]

Zhou J, Parada LF. PTEN signaling in autism spectrum disorders. Curr Opin Neurobiol. 2012; 22:873–879. [PubMed: 22664040]

Highlights

- NPAS1 represses cortical interneuron generation, regulating excitation/inhibition
- NPAS1 represses an enhancer of *Arx*, which mediates proliferation of CGE progenitors
- NPAS1&3 transcription factors have opposite roles in regulating interneuron number

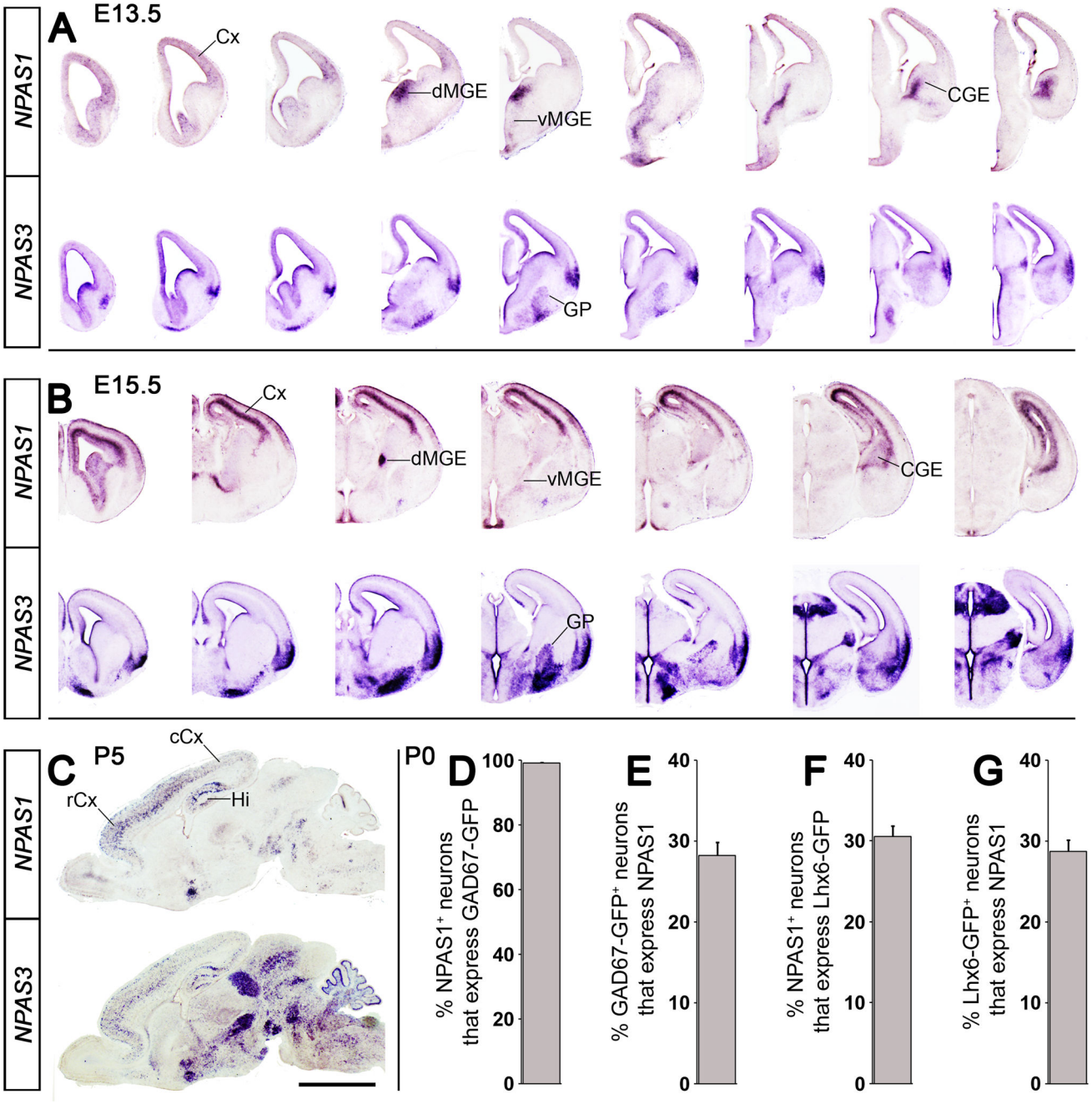

Figure 1. Forebrain expression of mouse *NPAS1* and *NPAS3* during embryonic and neonatal stages

(**A** and **B**) ISH on rostro-caudal series of coronal hemisections at E13.5 (A) and E15.5 (B). Note strong *NPAS1* expression in dMGE and CGE. (**C**) ISH on neonatal sagittal sections at P5. Note the rostral bias of cortical expression. (**D** to **G**) Quantification of percentage of NPAS1^{+} (immuno-stained) cortical interneurons (GAD67-GFP^{+} and Lhx6-GFP^{+}) at P0. *n* = 3 animals for (D) to (G). Abbreviations: CGE: caudal ganglionic eminence, Cx: cortex (rCX: rostral, cCx: caudal), GP: globus pallidus, Hi: hippocampus, MGE: medial ganglionic

eminence (dMGE: dorsal, vMGE: ventral). Scale bar, (A) 1.21 mm; (B) 1.74 mm; (C) 3 mm. See also Figure S1 and S2.

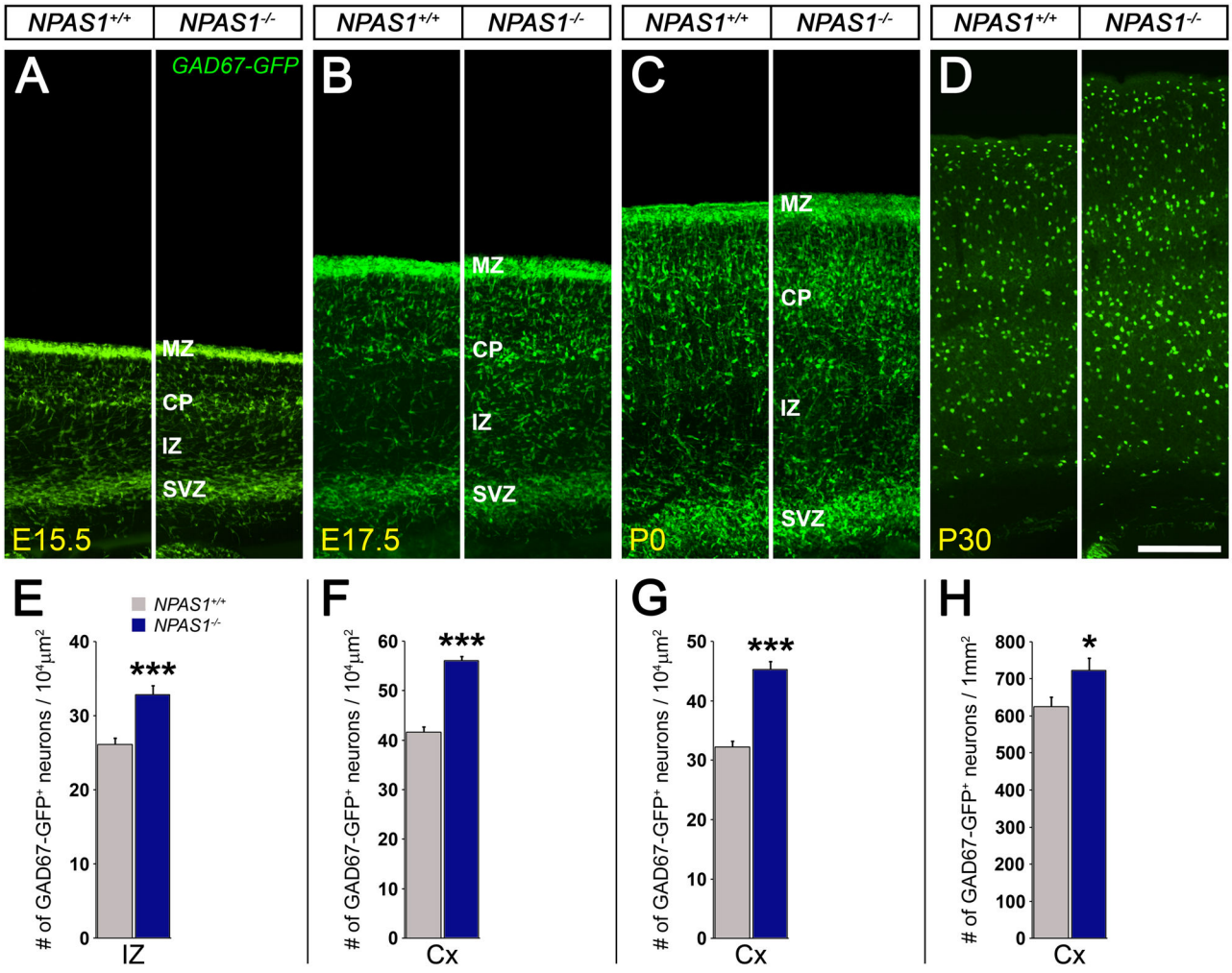

Figure 2. *NPAS1*$^{-/-}$ mice have increased numbers and density of GAD67-GFP^{+} cortical interneurons

(**A** to **D**) Increase in GAD67-GFP^{+} cortical interneurons (somatosensory Cx) beginning by E15.5 shown on coronal cortical sections at E15.5 (A), E17.5 (B), P0 (C) and P30 (D) in *NPAS1*$^{-/-}$ mice. (**E** to **H**) Quantification of GAD67-GFP^{+} neurons/10^4 µm^2 at E15.5 (E), E17.5 (F), P0 (G), and GAD67-GFP^{+} neurons/1 mm^2 at P30 (H). *n* = 3 animals per genotype for (E) to (H). Abbreviations: CP: cortical plate, Cx: cortex, IZ: intermediate zone, MZ: marginal zone, SVZ: subventricular zone. *P<0.05. ***P< 0.001. Scale bar, (A) to (C) 200 µm; (D) 400 µm. See also Figure S3.

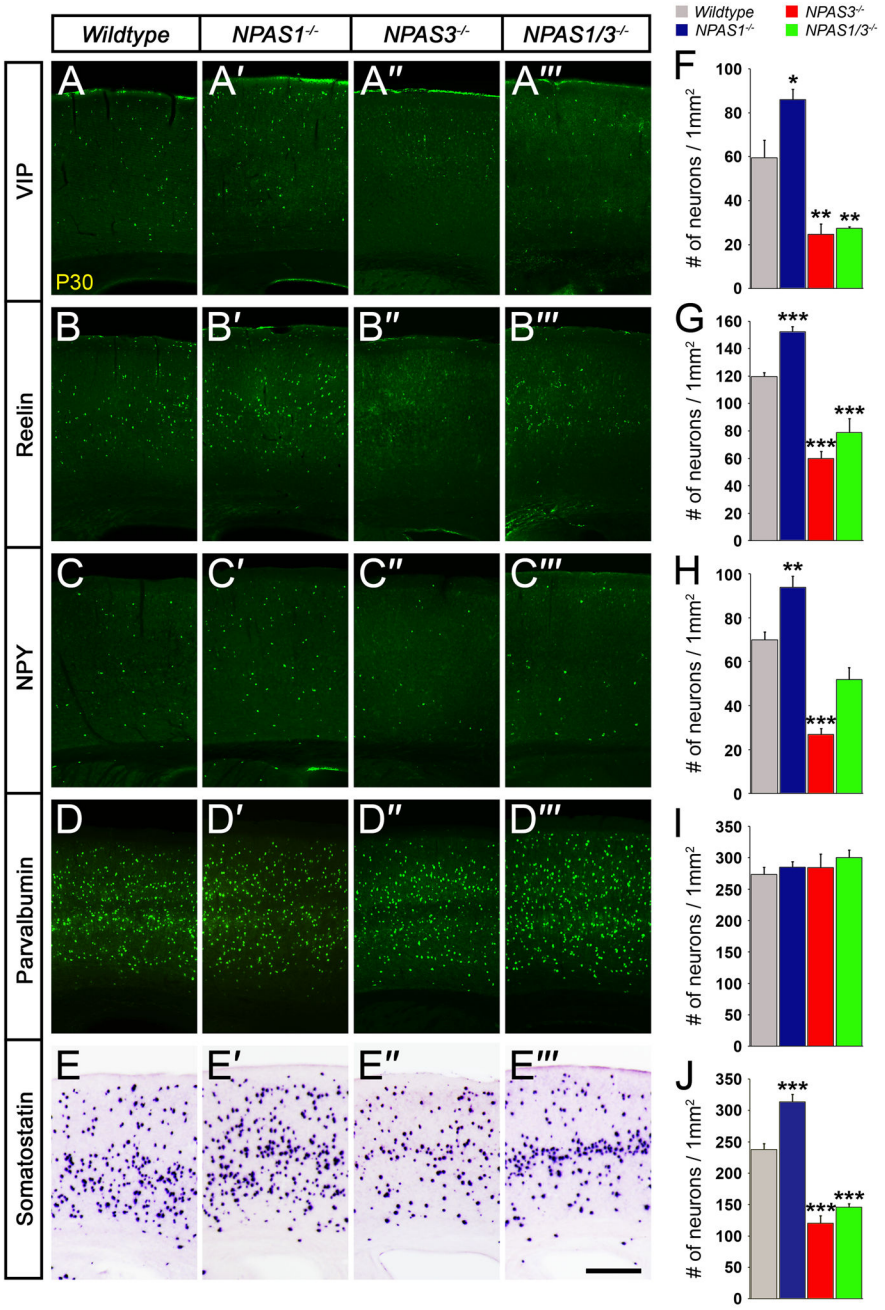

Figure 3. *NPAS1*$^{-/-}$ mice have increased, whereas *NPAS3*$^{-/-}$ and *NPAS1/3*$^{-/-}$ mice have decreased cortical interneurons

(**A** to **E‴**) Interneurons expressing VIP, reelin, NPY and somatostatin are increased in *NPAS1*$^{-/-}$ mice, but decreased in *NPAS3*$^{-/-}$ and *NPAS1/3*$^{-/-}$ mice. All mutants have a normal density of parvalbumin^{+} interneurons. Immunofluorescence staining of coronal neocortical sections (somatosensory Cx) at P30. (**F** to **J**) Quantification of VIP^{+} (F), reelin^{+} (G), NPY^{+} (H), parvalbumin^{+} (I), and somatostatin^{+} (J) neurons/1 mm^{2}. *n* = 3 animals per genotype for (F) to (J). *P<0.05. ***P< 0.001. Scale bar, (A) to (E‴) 400 μm.

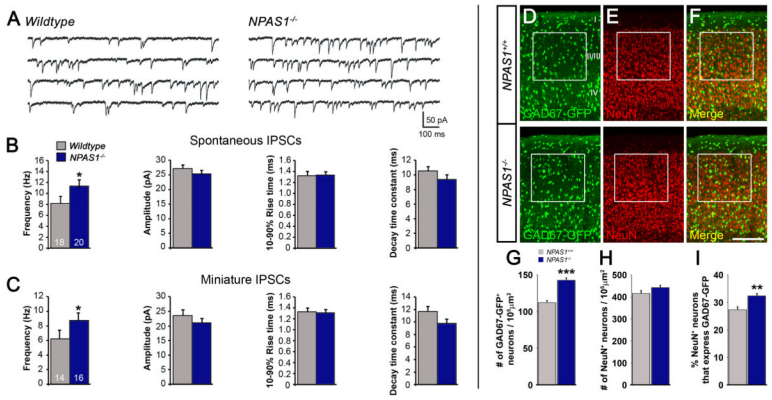

Figure 4. Synaptic inhibition to neocortical pyramidal cells is increased in *NPAS1*$^{-/-}$ mice

(**A**) Representative traces of sIPSCs recorded from layer II/III pyramidal neurons in somatosensory neocortex of wildtype and *NPAS1*$^{-/-}$ mice. (**B** and **C**) Mean sIPSC (B) and mIPSC (C) frequencies were higher in pyramidal neurons recorded from *NPAS1*$^{-/-}$ mice than in controls. Numbers of recorded cells are shown in each bar. No significant changes in sIPSC or mIPSC amplitude, 10–90% rise time, or decay time constant were detected. For (B) and (C), n = 7 wildtype and 9 *NPAS1*$^{-/-}$ animals. (**D** to **F**) Increase in GAD67-GFP^{+} interneurons (D) and percenta bge of neurons (NeuN^{+}) that are inhibitory (GAD67-GFP^{+}) (F) within layer II/III of *NPAS1*$^{-/-}$ somatosensory cortex (white boxes) shown on coronal sections at P21. The density of NeuN^{+} cells within layer II/III is not significantly increased in *NPAS1*$^{-/-}$ mutants (E). (**G** to **I**) Quantification of GAD67-GFP^{+} (G) and NeuN^{+} (H) neurons/10^5 µm^2 and percentage of NeuN^{+} cells that express *GAD67-GFP* within that area (I). n = 3 animals per genotype for (G) to (I). *P<0.05. **P<0.01. ***P< 0.001. Scale bar, (D) to (F) 200 µm. See also Figure S4.

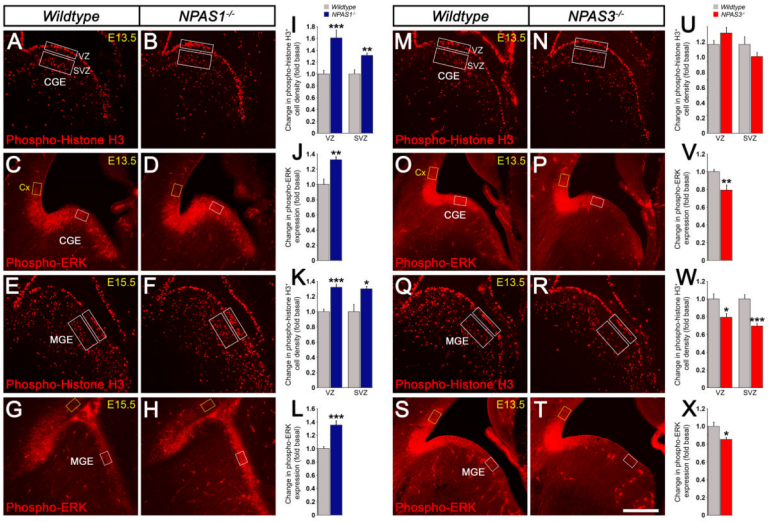

Figure 5. *NPAS1*$^{-/-}$ progenitors have increased proliferation and MAP kinase activity, while *NPAS3*$^{-/-}$ progenitors exhibit decreased proliferation and MAP kinase activity

(**A** to **H**) Immunofluorescence assays of coronal sections demonstrate increased proliferation (phospho-histone H3^{+} M-phase cells) and MAP kinase activity (phospho-ERK) in the E13.5 CGE (A to D), and E15.5 MGE (E to H) of *NPAS1*$^{-/-}$ progenitors. (**I** to **L**) Quantification of phospho-histone H3^{+} (I and K) cells and phospho-ERK (J and L) levels in *NPAS1*$^{-/-}$ mutants. *n* = 3 animals per genotype for (I) to (L). (**M** to **T**) *NPAS3*$^{-/-}$ progenitors display reduced proliferation and MAP kinase activity in the E13.5 MGE (Q to T). While MAP kinase activity was decreased in the E13.5 CGE (O to P), proliferation of progenitors was unaltered in the E13.5 CGE (M to N) of *NPAS3*$^{-/-}$ mutant mice. (**U** to **X**) Quantification of phospho-histone H3^{+} (U and W) cells and phospho-ERK (V and X) levels in *NPAS3*$^{-/-}$ mutants. Proliferation was measured in the VZ and SVZ (white boxes). Phospho-ERK levels in the CGE/MGE (white box) were normalized by comparison with cortical levels (yellow box). *n* = 3 animals per genotype for (U) to (X). Abbreviations: CGE: caudal ganglionic eminence, Cx: cortex, MGE: medial ganglionic eminence, SVZ: subventricular zone, VZ: ventricular zone. *P<0.05. **P<0.01. ***P< 0.001. Scale bar, (A) to (H) and (M) to (T) 250 μm. See also Figure S5.

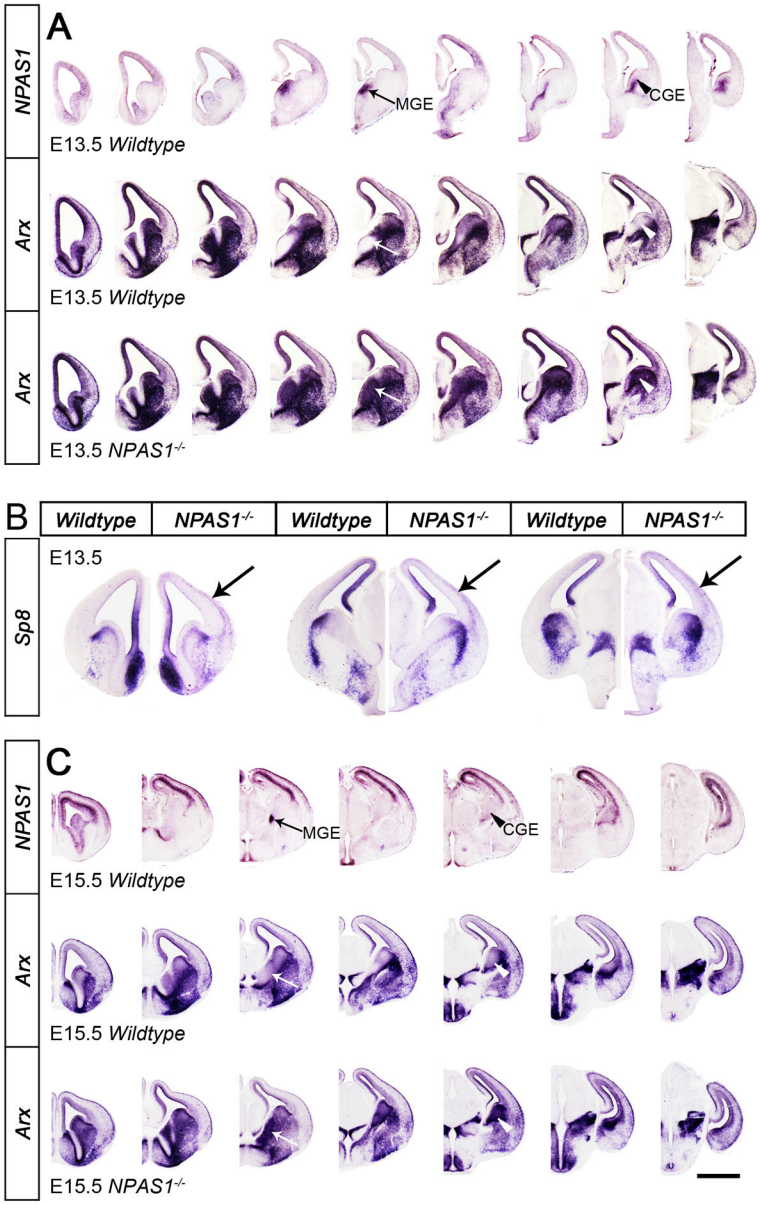

Figure 6. *NPAS1*$^{-/-}$ GEs have increased *Arx* expression, whereas *NPAS1*$^{-/-}$ cortices reveal increased Sp8 expression

(**A**) ISH assay on coronal hemisections arrayed in a rostro-caudal series reveal that *NPAS1*$^{-/-}$ progenitors have increased *Arx* expression in the VZ/SVZ regions of the E13.5 MGE (arrows) and CGE(arrowheads) [compare white arrow and arrowhead in bottom tier (*NPAS1*$^{-/-}$) to middle tier (wildtype)] where *NPAS1* is expressed (black arrow and arrowhead in top tier). (**B**) At E13.5, Sp8 expression appears increased in a pattern consistent with tangentially migrating cortical interneurons (arrows). Data presented in coronal sections at three rostro-caudal planes (left to right). (**C**) ISH assay on coronal hemisections displayed in a rostro-caudal series show that *NPAS1*$^{-/-}$ progenitors have increased *Arx* expression in the VZ/SVZ regions of the E15.5 MGE (arrows) and CGE(arrowheads) [compare white arrow and arrowhead in bottom tier (*NPAS1*$^{-/-}$) to

middle tier (wildtype)] where *NPAS1* is expressed (black arrow and arrowhead in top tier). Abbreviations: CGE: caudal ganglionic eminence, MGE: medial ganglionic eminence. Scale bar, (A) 1 mm; (B) 723 μm; (C) 1.25 mm. See also Figure S6.

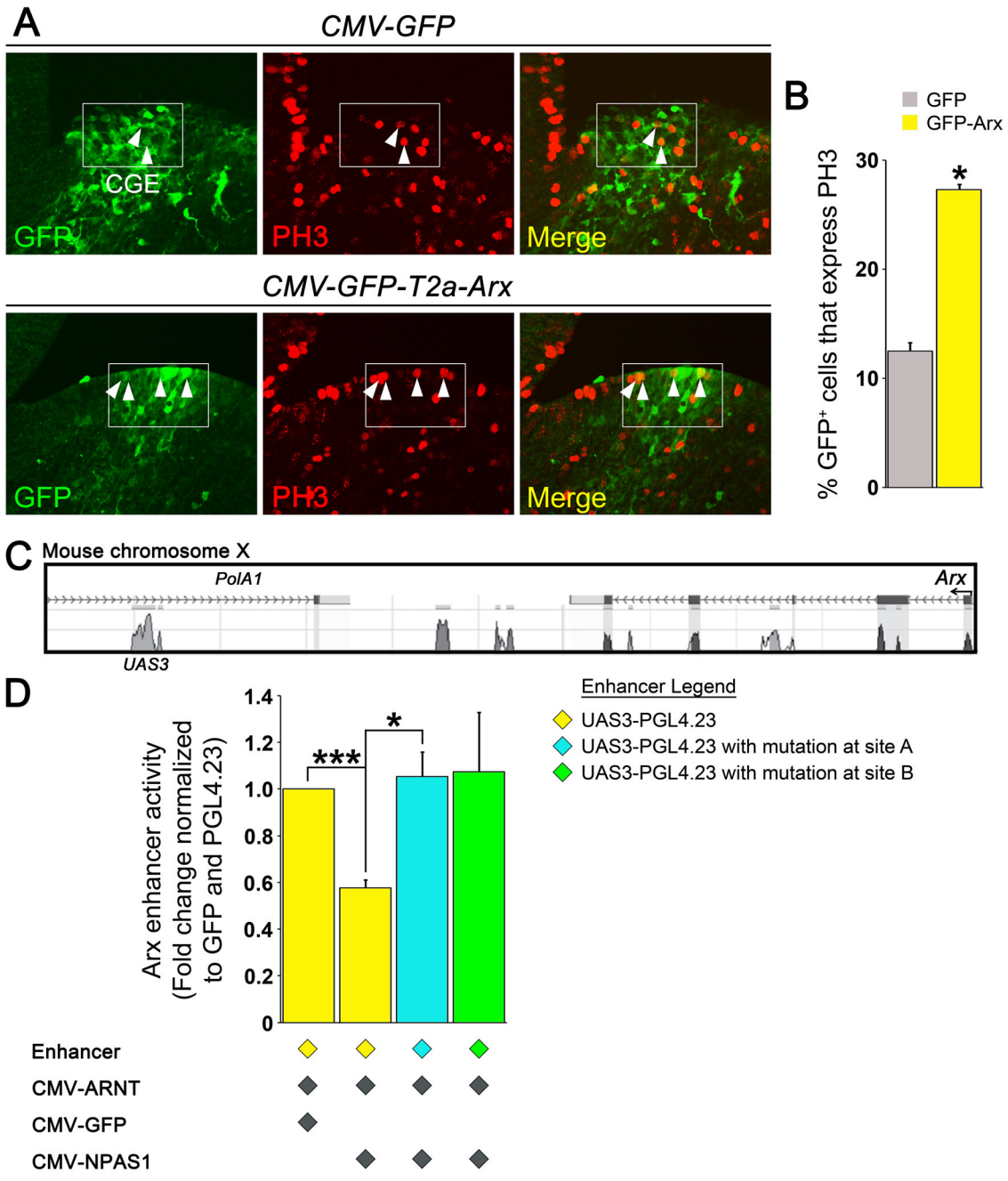

Figure 7. Increased *Arx* expression in the CGE mediates increased subpallial proliferation

(**A** and **B**) *In utero* lentiviral transduction of *Arx* into the E13.5 CGE results in increased cell proliferation (PH3). Arrowheads in (A) indicate $GFP^+/PH3^+$ cells. *n* = 3 animals per experimental condition for (B). (**C**) *Arx* locus on mouse X chr, showing evolutionarily conserved domains, one of which is a subpallial enhancer (*UAS3*) (Colasante et al., 2008; Visel et al., 2013) that has two predicted *NPAS1/ARNT* sites (Figure S6). (**D**) Transcription assay of E12.5 CGE primary culture shows that *NPAS1/ARNT* expression represses activity of the *Arx* subpallial enhancer. Mutation of the *Arx* enhancer at site A, but not site B, resulted in a rescue of the repression induced by *NPAS1/ARNT*. *n* = 3 independent

experiments, each performed in triplicate for (D). Abbreviations: CGE: caudal ganglionic eminence. *P<0.05. **P<0.01. Scale bar, (A) 70 μm. See also Figure S7.